








Synergistic substrate cofeeding stimulates reductive metabolism

Junyoung O. Park ^{1,5,7}, Nian Liu ^{1,7}, Kara M. Holinski¹, David F. Emerson ¹, Kangjian Qiao¹, Benjamin M. Woolston ¹, Jingyang Xu^{1,2}, Zbigniew Lazar ^{1,3}, M. Ahsanul Islam ^{1,6}, Charles Vidoudez⁴, Peter R. Girguis⁴ and Gregory Stephanopoulos ^{1*}

Advanced bioproduct synthesis via reductive metabolism requires coordinating carbons, ATP and reducing agents, which are generated with varying efficiencies depending on metabolic pathways. Substrate mixtures with direct access to multiple pathways may optimally satisfy these biosynthetic requirements. However, native regulation favouring preferential use precludes cells from co-metabolizing multiple substrates. Here we explore mixed substrate metabolism and tailor pathway usage to synergistically stimulate carbon reduction. By controlled cofeeding of superior ATP and NADPH generators as ‘dopant’ substrates to cells primarily using inferior substrates, we circumvent catabolite repression and drive synergy in two divergent organisms. Glucose doping in *Moorella thermoacetica* stimulates CO₂ reduction (2.3 g CDW⁻¹ h⁻¹) into acetate by augmenting ATP synthesis via pyruvate kinase. Gluconate doping in *Yarrowia lipolytica* accelerates acetate-driven lipogenesis (0.046 g CDW⁻¹ h⁻¹) by obligatory NADPH synthesis through the pentose cycle. Together, synergistic cofeeding produces CO₂-derived lipids with 38% energy yield and demonstrates the potential to convert CO₂ into advanced bioproducts. This work advances the systems-level control of metabolic networks and CO₂ use, the most pressing and difficult reduction challenge.

One of the greatest feats of metabolism is the ability to synthesize reduced compounds from input substrates with varying oxidation states. Using reductive metabolism, cells reassemble the output of substrate catabolism for energy-dense bioproduct synthesis¹. This process is often implemented in both laboratory and industry with single organic carbon sources (for example, sugars) as inputs due to simplicity^{2,3}. Nonetheless, single substrates naturally impose stoichiometric constraints on available carbons, energy and redox cofactors, leading to biosynthetic imbalance and suboptimal product yield. Thus, genetic rewiring of metabolic pathways is required to advantageously shift these stoichiometries⁴, which precludes wide application of non-model organisms that lack suitable genetic tools⁵.

Substrate mixtures, on the other hand, present the potential to alleviate such stoichiometric constraints in reductive metabolism without genetic rewiring. Since each substrate has unique efficiencies for carbon, energy and cofactor generation, varying the relative amounts of substrates in the mixture allows fine-tuning of carbon-to-energy-to-cofactor ratios. Furthermore, substrates with different entry points to metabolism alleviate protein burdens by providing the required components in fewer enzymatic steps. Nevertheless, mixed substrate metabolism is epitomized by sequential (for example, diauxie) and hierarchical (yet simultaneous) use based on substrate preference^{6–8}, reflecting the evolutionary fitness of cells in their native environments⁹. Despite the recent success of substrate mixture batch fermentation using limited substrate pairs (that do not trigger catabolite repression)^{10,11}, genetic engineering^{12,13} and directed evolution^{14–16}, the full mixture spectrum remains inaccessible and thus unexplored.

In the present study, we report a simple and universal solution to overcoming undesirable substrate preferences and improving carbon reduction in various organisms. We eliminate catabolite repression by controlling the continuous feed rate of preferred superior substrates to maintain negligible concentrations in systems dominated by inferior substrates. Using this method, we explored mixed substrate metabolism and therein observed enhanced metabolic productivity that exceeds the sum of individual substrate productivities.

This substrate cofeeding scheme was applied to two widely divergent organisms to optimize reductive metabolism of lipogenesis and acetogenesis. We cultured the oleaginous yeast *Yarrowia lipolytica* on acetate and continuously fed limiting quantities of glucose, fructose, glycerol or gluconate as ‘dopant’ substrates to augment reductive metabolism. In this fed-batch set-up, cells simultaneously consumed acetate and the supplemented substrate, with acetate remaining as the primary carbon source. In particular, the rate of lipogenesis with gluconate doping was twice as fast as that of the acetate-only control. Tracing ¹³C from gluconate revealed that obligatory NADPH synthesis by recursive use of the oxidative pentose phosphate pathway (PPP) was responsible for the observed synergy with acetate.

We then set out to source acetate via acetogenesis, a reductive metabolic process starting from CO₂. The acetogenic bacterium *Moorella thermoacetica* simultaneously consumes CO₂ and glucose with the latter providing both ATP and electrons (e⁻) necessary for CO₂ fixation, cell maintenance and growth¹⁷. However, tracing ¹³C-labelled glucose revealed that glucose metabolism dominated and e⁻ generation was coupled to undesirable decarboxylation.

¹Department of Chemical Engineering, Massachusetts Institute of Technology, Cambridge, MA, USA. ²Key Laboratory of Drug Prevention and Control Technology of Zhejiang Province, Zhejiang Police College, Hangzhou, China. ³Department of Biotechnology and Food Microbiology, Wrocław University of Environmental and Life Sciences, Monskiego, Wrocław, Poland. ⁴Department of Organismic and Evolutionary Biology, Harvard University, Cambridge, MA, USA. ⁵Present address: Department of Chemical and Biomolecular Engineering, University of California, Los Angeles, Los Angeles, CA, USA. ⁶Present address: Department of Chemical Engineering, Loughborough University, Loughborough, UK. ⁷These authors contributed equally: Junyoung O. Park, Nian Liu. *e-mail: gregstep@mit.edu

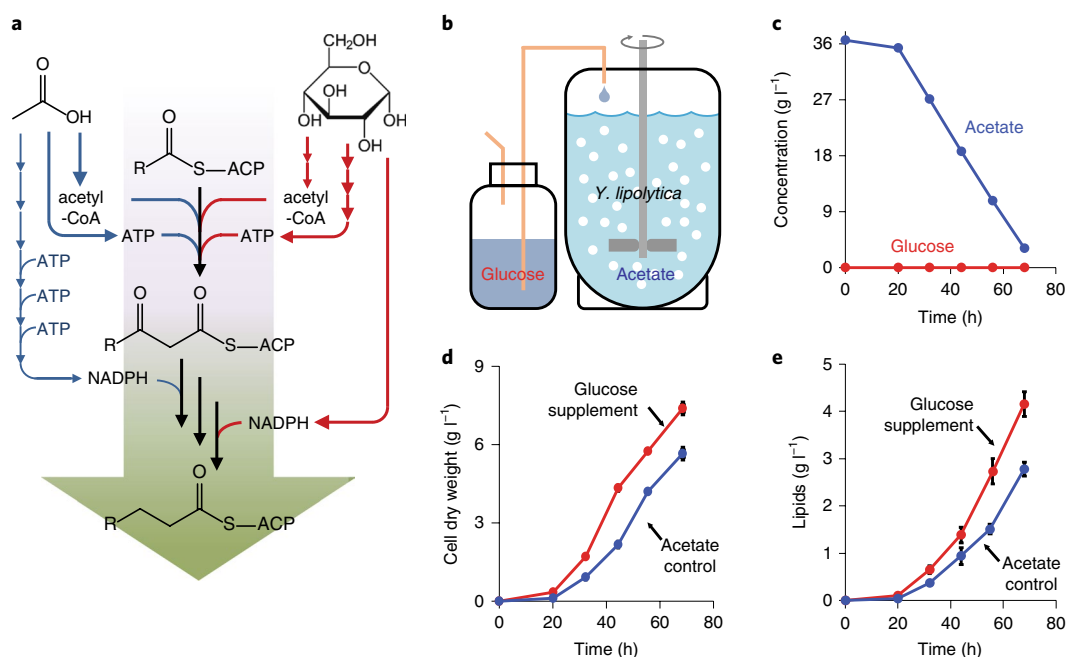


Fig. 1 | Continuous glucose cofeeding relieves repression of acetate in *Y. lipolytica*. **a**, Acetate can efficiently support acetyl-CoA and ATP generation through the TCA cycle but not NADPH generation, which requires many enzymatic steps and ATP. Glucose, on the other hand, can produce NADPH more directly through oxidative PPP. **b**, Since glucose batch feeding suppresses acetate consumption, glucose was continuously supplemented in small quantities to the acetate culture. **c**, Despite the continuous feeding of glucose, its concentration in the reactor remained at 0 and acetate concentration decreased. Thus, the fed-batch system enabled simultaneous consumption of acetate and glucose. **d,e**, Biomass (**d**) and lipid production (**e**) were faster and higher with glucose ‘doping’ compared to the acetate-only control. **c–e**, The centre and error bars represent the mean \pm s.e.m. ($n=3$ biologically independent samples).

To shift cellular metabolism towards greater CO_2 incorporation, we designed a chemostat that continuously supplied limiting glucose and ample H_2 . Under these conditions, CO_2 reduction metabolism dominated, glucose primarily produced ATP sufficient for cell maintenance via pyruvate kinase and carbon-free e^- for net CO_2 reduction were supplied by H_2 . Importantly, with dopant substrate glucose, *M. thermoacetica* rapidly converted CO_2 into acetate exclusively, serving as the ideal input for gluconate-doped lipogenesis.

With the aforementioned synergy, we fixed CO_2 at 2.3 g per g cell dry weight per hour ($\text{g gCDW}^{-1} \text{h}^{-1}$), substantially faster than approximately $0.05 \text{ gCDW}^{-1} \text{h}^{-1}$ of typical photosynthetic systems¹⁸. Using the resulting acetate, we produced lipids at $0.046 \text{ gCDW}^{-1} \text{h}^{-1}$, a more than twofold improvement over the previously optimized system (approximately $0.02 \text{ gCDW}^{-1} \text{h}^{-1}$)¹⁹. Coordinating the glucose-doped acetogenesis and gluconate-doped lipogenesis, we converted carbons in the most oxidized, undesirable state (CO_2) to the reduced, energy-dense state (lipids) with 38% energy yield. Through synergistic substrate cofeeding, we overcame the limitation of ATP- and NADPH-dependent biological carbon reduction, paving the path for CO_2 -derived advanced bioproduct synthesis.

Accelerating lipogenesis from acetate by enhancing NADPH generation in *Y. lipolytica*

Lipogenesis requires a balanced supply of acetyl coenzyme A (acetyl-CoA), ATP and NADPH at an approximately 1:1:2 ratio. Single substrates, such as glucose and acetate, can provide all three building blocks for lipids^{19–21}. However, lipid synthesis from acetate, despite acetate’s direct contribution to acetyl-CoA and ATP, is slower compared to that from glucose²² (Fig. 1a). This is because in *Y. lipolytica*, NADPH generation is mainly through oxidative PPP, which takes a series of ATP-intensive reactions to arrive at, starting from acetate²³.

We aimed to enhance acetate-to-lipid conversion by better supplying NADPH. Since glucose can flow more directly into oxidative PPP than acetate, we provided both acetate and glucose to a *Y. lipolytica* batch culture. Consistent with the widely accepted phenomenon of catabolite repression²⁴, cells consumed glucose only at first (Supplementary Fig. 1). To overcome this selective preference (that is, diauxie), we devised a fed-batch system, where instead the same amount of glucose was continuously supplied over the course of fermentation to an acetate culture (Fig. 1b). The feed rate was kept slow to maintain negligible glucose concentrations in the reactor. In this set-up, despite constant introduction of glucose, we observed steadily decreasing acetate and no glucose in the reactor, suggesting simultaneous consumption of the two carbon sources (Fig. 1c). Furthermore, the fed-batch cofeeding strategy enhanced both growth and lipid production in *Y. lipolytica* significantly compared to the acetate-only control (Fig. 1d,e).

Using the same fed-batch system, we also tested supplementing other substrates (fructose, glycerol and gluconate) that enter metabolism near oxidative PPP as metabolic ‘dopants’ to provide NADPH (Fig. 2a). In all cases, we observed simultaneous consumption of acetate and the supplemented substrate (Supplementary Fig. 2). As with glucose, cell growth and lipid production were enhanced (Supplementary Fig. 3) despite the supplemental substrates constituting only small fractions of carbons (Fig. 2b). To distinguish whether the increase in lipid production was due to cellular metabolism enhancements or simply having more cells in the culture, we determined specific growth rates and productivities. Substrate doping nearly doubled both the specific growth rate (Fig. 2c) and the specific lipid productivity during the nitrogen-replete growth phase (Fig. 2d). In the nitrogen-depleted lipogenic phase, glucose, fructose and glycerol cofeeding only modestly enhanced specific productivity, while gluconate cofeeding significantly outperformed all other conditions (Fig. 2e).

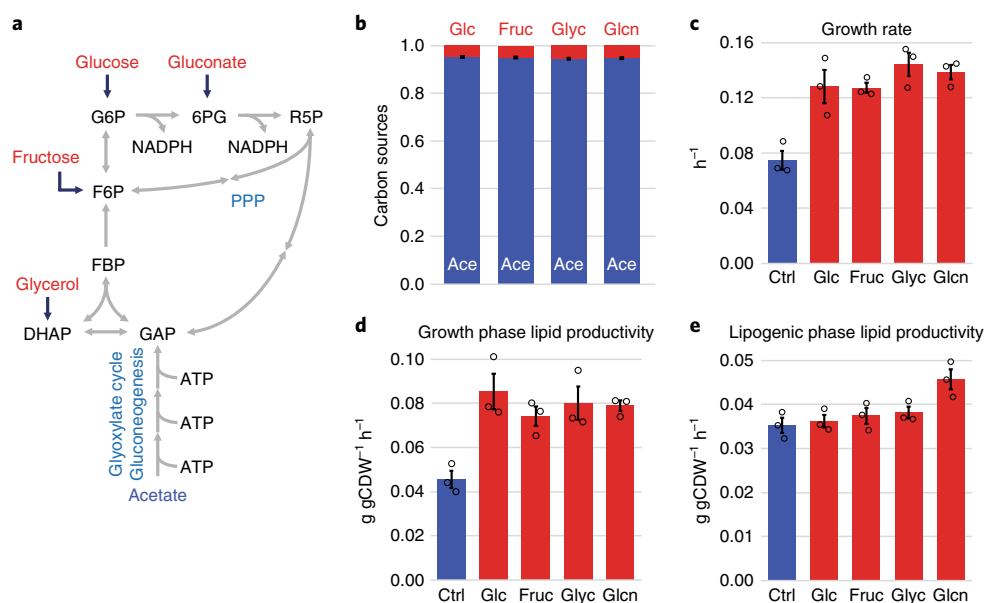


Fig. 2 | Cofeeding substrates near the oxidative PPP accelerates cell growth and lipogenesis from acetate. **a**, Glucose, fructose, glycerol and gluconate enter central carbon metabolism through upper glycolysis and PPP. DHAP, dihydroxyacetone phosphate; FBP, fructose 1,6-bisphosphate; GAP, glyceraldehyde 3-phosphate. **b**, Supplementation of these four substrates accounted for approximately 5% of the total carbon consumed by the cells; the primary carbon source was acetate. **c**, Specific growth rates nearly doubled with substrate cofeeding compared to the acetate-only control. **d**, Growth phase (nitrogen-replete) specific lipid productivity nearly doubled with substrate cofeeding. **e**, Lipogenic phase (nitrogen-depleted) specific lipid productivity was mildly enhanced by glucose, fructose or glycerol supplementation. Gluconate ‘doping’ significantly outperformed the other conditions. **b–e**, The centre and error bars represent the mean \pm s.e.m. ($n=3$ biologically independent samples). Individual data points for each biological replicate are shown as circles.

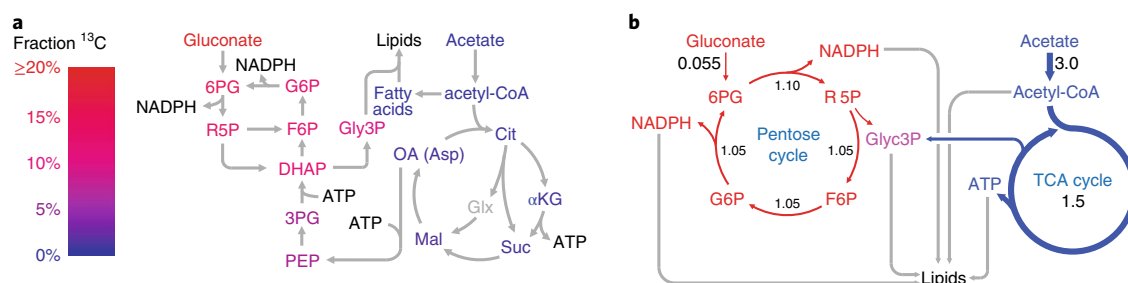


Fig. 3 | Gluconate generates NADPH via the pentose cycle. **a**, Tracing carbons from $[U-^{13}C_6]$ gluconate revealed partitioned use of metabolism. The heavy ^{13}C of gluconate remained mainly in upper glycolysis and PPP. Acetyl-CoA and TCA intermediates were completely unlabelled, indicating exclusive contribution from acetate. α KG, α -ketoglutarate; Glyc3P, glycerol 3-phosphate; Mal, malate; OA, oxaloacetate; Suc, succinate. **b**, Metabolic flux analysis via isotope mass balancing revealed the cyclic reaction sequence generating NADPH. The ‘pentose cycle’ consisted of the NADPH-producing oxidative PPP, transketolase, transaldolase and phosphoglucose isomerase. Flux values are in $\text{mmol gCDW}^{-1} \text{h}^{-1}$.

Recursive NADPH generation via the pentose cycle

To understand the mechanism of accelerated lipid production, we aimed to elucidate how continuous gluconate supplementation rewires metabolism. Tracing the carbons from $[U-^{13}C_6]$ -gluconate by liquid chromatography–mass spectrometry (LC–MS), we observed that the ^{13}C atoms were confined to the PPP and upper glycolysis (Fig. 3a and Supplementary Table 1). Gluconate enters metabolism as 6-phosphogluconate (6PG), which can go only in the oxidative direction through oxidative PPP because the combined thermodynamics of glucose-6-phosphate dehydrogenase and 6-phosphogluconolactonase ($\Delta G^{\circ} = -29 \text{ kJ mol}^{-1}$) strongly favours the flow of 6PG further into the PPP²⁵. This causes gluconate to obligatorily generate NADPH via 6PG dehydrogenase, which is probably responsible for the acceleration of lipogenesis. On the other hand, metabolites in the tricarboxylic acid (TCA) cycle, as

well as fatty acids, were completely unlabelled, indicating exclusive contribution of lipogenic acetyl-CoA and ATP from acetate (Fig. 3a and Supplementary Table 1). These labelling data suggested the partitioned usage of metabolism, where acetate primarily provided acetyl-CoA and ATP while gluconate primarily provided NADPH to meet the metabolic demands of lipogenesis.

To further validate the hypothesis that gluconate enhances lipogenesis through NADPH supplementation, we performed metabolic flux analysis using the labelling data, substrate uptake rates and lipid production rate. The flux distribution that best fitted all these measurements revealed a strong flux through the oxidative PPP NADPH-generating steps (Fig. 3b and Supplementary Table 2). Interestingly, phosphoglucose isomerase operated in the reverse direction converting fructose 6-phosphate (F6P) to glucose 6-phosphate (G6P). Flux analysis also revealed that the gluconeogenic,

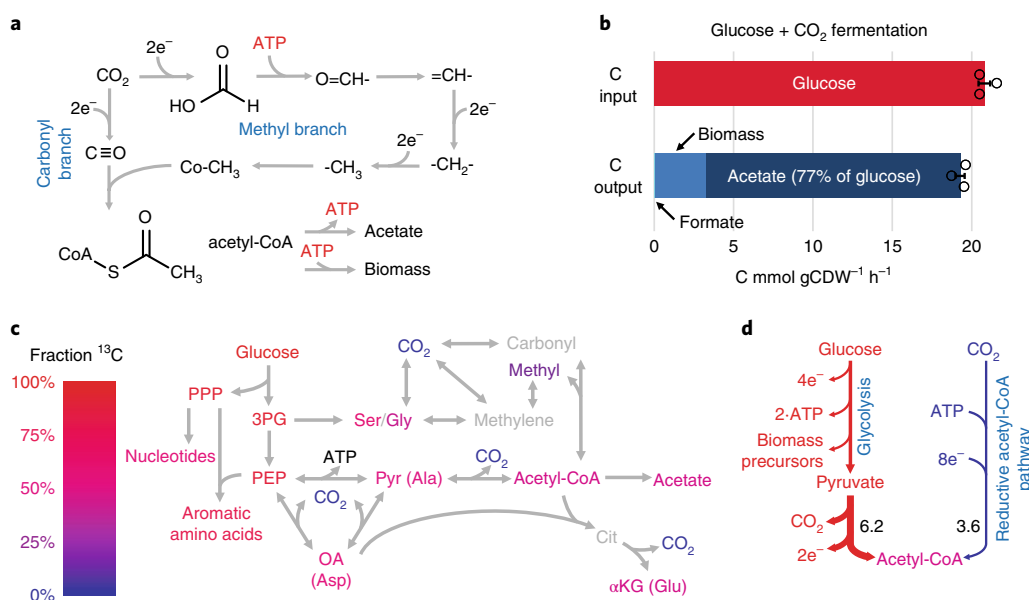


Fig. 4 | Glucose generates ATP for CO₂ fixation but leads to decarboxylation in *M. thermoacetica*. **a**, The reductive acetyl-CoA pathway consists of the carbonyl and methyl branches for conversion of CO₂ into the acetyl group. The methyl branch requires ATP. **b**, Analysis of carbon input and output in batch cofeeding of *M. thermoacetica* with glucose and CO₂ revealed the preferential use of glucose. The centre and error bars represent the mean \pm s.e.m. ($n=3$ biologically independent samples). Individual data points for each biological replicate are shown as circles. **c**, Batch cofeeding [¹³C₆]glucose and CO₂ revealed the simultaneous use of glucose and CO₂. Glucose carbons contributed mainly to glycolysis and PPP while partially to the TCA cycle. A substantial fraction of TCA carbons was traced to CO₂. **d**, Despite simultaneous use of CO₂, preferred glucose use led to undesirable decarboxylation outpacing CO₂ uptake. Flux values are in mmol gCDW⁻¹ h⁻¹ of acetyl-CoA.

oxidative PPP and non-oxidative PPP fluxes together form a metabolic cycle, which we termed the ‘pentose cycle’ (Fig. 3b and Supplementary Table 2). Akin to the TCA cycle, the pentose cycle recursively oxidized the carbons from gluconate into CO₂ while preserving the electrons as NADPH for lipogenesis, maximizing the dopant substrate’s role as an NADPH provider.

Preferential use of glucose leads to excessive decarboxylation in CO₂-fixing *M. thermoacetica*

Acetogenesis is a reductive metabolic process that produces acetate from CO₂. In acetogenic organisms, the reductive acetyl-CoA pathway incorporates CO₂ as the carbonyl and methyl components of the acetyl group²⁶ (Fig. 4a). The methyl branch of this pathway requires ATP, which acetogens may recover by acetate production. This ATP conservation contributes to efficient autotrophic CO₂ fixation²⁷; however, autotrophic culture conditions, which derive energy solely from inorganic sources (for example, oxidation of H₂), result in slow metabolism and low culture density^{28,29}.

Since glycolysis effectively produces ATP and the e⁻ necessary for operating the reductive acetyl-CoA pathway, we cofed CO₂ and [U-¹³C₆]-glucose to *M. thermoacetica* and looked for signs of CO₂ incorporation. If acetate were the only product, we would expect up to 100% carbon yield, that is, three acetate molecules per glucose²⁹. On the other hand, with potential other products (for example, pyruvate) or biomass components (for example, Ser/Gly, Asp and Glu), net CO₂ use becomes feasible since some pathways generate reducing agents without CO₂ production or fix more CO₂ than the amount produced (Supplementary Fig. 4). Since net CO₂ use depends on the types and fractions of fermentation products, we quantified cell growth, the secreted molecules and their carbon yields relative to glucose consumption (Fig. 4b). We observed the activity of the reductive acetyl-CoA pathway since the produced acetate accounted for 77% of glucose carbons, exceeding what is possible via glycolysis (67%). However, since the glucose carbon consumption rate approximately matched the total carbon output

rate of major products (that is, biomass, acetate and formate accounted for 93%), we did not observe net CO₂ use.

We hypothesized that our observed carbon yield was due to insufficient reducing agents available for new CO₂ use and cells preferentially consuming glucose over CO₂. To trace the fate of ¹³C-glucose carbons and to visualize metabolic pathway use, we measured ¹³C enrichment in cellular metabolites with LC-MS. Unlabelled CO₂ was provided in the headspace and CO₂ remained mostly unlabelled (Supplementary Fig. 5). The carbons of glycolytic intermediates were $\geq 90\%$ labelled except for pyruvate, which was approximately 50% labelled (Fig. 4c and Supplementary Table 3). The lower labelling in pyruvate was due to reversible pyruvate:ferredoxin oxidoreductase (PFOR), which can form pyruvate by combining unlabelled CO₂ and the acetyl group derived from the reductive acetyl-CoA pathway. With phosphoenolpyruvate (PEP) remaining mostly labelled, the contrasting pyruvate labelling indicated that pyruvate kinase (PEP + ADP \rightarrow pyruvate + ATP) was forward-driven to produce ATP.

Interestingly, serine, glycine and other amino acids derived from pyruvate and TCA cycle intermediates were also half-labelled (Fig. 4c and Supplementary Table 3). These labelling data suggested shared usage of central metabolism, where glucose and CO₂ jointly contributed to the TCA cycle (and thus to non-aromatic amino acid biosynthesis). However, because glycolysis and the PPP (and thus the synthesis of nucleotide ribose rings and aromatic amino acids) were driven mainly by glucose, cells incorporated more carbons from glucose. Therefore, despite the simultaneous consumption of CO₂ and glucose, lack of observable net CO₂ fixation was the result of cells prioritizing ATP production and cell growth. Prioritizing ATP production involves faster glycolysis via faster glucose uptake. This substrate hierarchy favouring glucose subsequently led to excessive pyruvate decarboxylation via PFOR (Fig. 4d and Supplementary Table 4), which, together with CO₂-producing biosynthetic pathways (Supplementary Fig. 6), outpaced CO₂ incorporation.

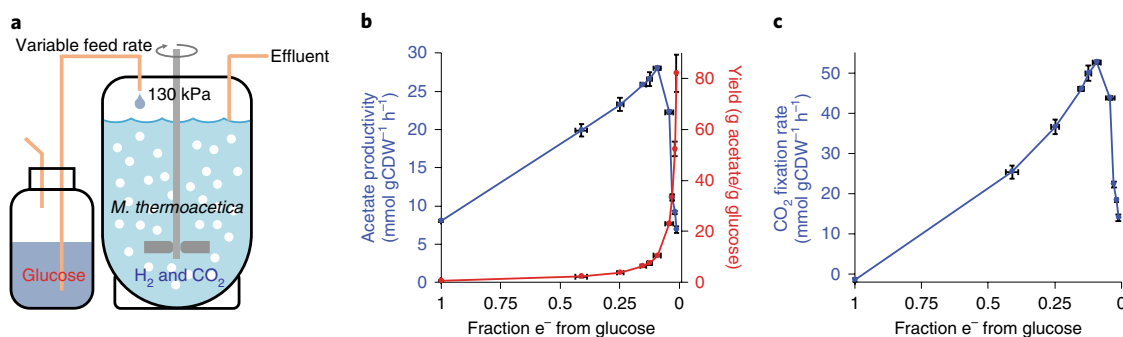


Fig. 5 | Continuous glucose cofeeding accelerates acetogenesis from CO₂ fixation at the autotrophic limit. a, Since glucose batch feeding leads to undesirable decarboxylation, glucose was continuously supplemented in small quantities to the gas-fermenting *M. thermoacetica* culture. **b,c**, Acetate productivity, yield and CO₂ fixation rate at varying fractions of electrons (e⁻) derived from glucose versus H₂. The plots include both batch and chemostat data (Supplementary Table 5). The centre and error bars represent the mean ± s.e.m. (*n* = 3 biologically independent samples). **b**, Acetate productivity peaked when 91% of e⁻ were derived from H₂ and 9% glucose. On the other hand, carbon yield (acetate produced per glucose consumed) increased with increasing fraction of e⁻ from H₂. **c**, CO₂ fixation rate peaked when 9% of e⁻ were derived from glucose and remained high near the autotrophic limit.

Accelerating acetate production from CO₂ by decoupling e⁻ supply from decarboxylation

Since undesirable decarboxylation is coupled to the PFOR step for e⁻ generation from glucose (two e⁻ generated per CO₂ released), we aimed to limit the function of glucose as an e⁻ source by decreasing PFOR flux and stimulating net CO₂ incorporation (four e⁻ required per CO₂ fixed). On the other hand, sufficient ATP is still required from glucose through pyruvate kinase to avoid slow metabolism and sustain CO₂ reduction. We note that acetate production via the reductive acetyl-CoA pathway does not consume ATP, leading to cell maintenance (that is, housekeeping) being the only ATP requirement for converting CO₂ to acetate (Supplementary Fig. 7). Hence, we implemented glucose-limiting culture environments in a chemostat to reduce the rate of glycolysis such that it supplies the required ATP but overall decarboxylation is slowed (Fig. 5a). To compensate for the decreased e⁻ availability, cells were provided with H₂ as a carbon-free e⁻ source that yields reducing agents without CO₂ generation. In addition, low dilution rates (< 0.1 h⁻¹) were selected to minimize biomass formation and maximize cell residence time in the reactor.

Using this glucose doping system, productivities and yields at various fractions of e⁻ derived from glucose versus H₂ were obtained (Fig. 5b). In this plot, we also included batch results with or without H₂ in the headspace (Supplementary Table 5). Interestingly, the presence of H₂ decreased the glucose consumption rate, shifting carbon substrate preferences towards CO₂ (Supplementary Fig. 8). At steady state, acetate concentration in the effluent from the chemostat could exceed 13 g l⁻¹. With decreasing fractions of e⁻ from glucose, the acetate production rate could be more than 80 times as fast as the glucose feed rate, and the carbon yield monotonically increased to >80 g acetate produced per g glucose consumed. This high yield indicated that the overwhelming majority of acetate and biomass was derived from CO₂ rather than glucose. While cell growth rates were slow in the chemostat (growth rate = dilution rate), acetate production remained fast (Fig. 5b). Importantly, we found that, at 2% of e⁻ from glucose, glucose doping simultaneously enabled a very high yield (>50 g acetate per g glucose) and substantial acetate productivity (>9 mmol gCDW⁻¹ h⁻¹, approximately 1/3 of the maximum observed productivity).

Across the glucose + H₂ energy landscape, CO₂ fixation rates peaked at 52.7 mmol gCDW⁻¹ h⁻¹ (2.3 g gCDW⁻¹ h⁻¹) (Fig. 5c). Such high rates implied that we not only decreased CO₂ generation from pyruvate decarboxylation but also increased the reductive acetyl-CoA pathway flux. Furthermore, the maximum rate occurring between the two extremes (glucose only and H₂ only) demonstrated

that the CO₂ fixation rate is determined by a balance between reducing agents and ATP supplied via H₂ and glucose, respectively. Thus, using controlled glucose doping, we decoupled e⁻ supply from decarboxylation, shifted cellular metabolism towards favouring CO₂ use over glucose and achieved rapid and continuous CO₂ conversion into acetate.

Coordination of 'doped' acetogenesis and lipogenesis

Coordinating acetogenesis and lipogenesis allows CO₂-to-acetate-to-lipid conversion. Interestingly, the observed acetate and fatty acid productivities from glucose and gluconate doping (*V*₁₂) exceeded not only the measured productivities with individual substrates (*V*₁ or *V*₂), but also the expected productivity for the two substrates combined (*V*₁ + *V*₂) (Fig. 6a). The expected productivity was extrapolated linearly from the combination of supplemental glucose feeding with CO₂ + H₂ batch fermentation for acetogenesis and the combination of supplemental gluconate feeding with acetate batch fermentation for lipogenesis (Supplementary Note).

We attributed the observed synergy (*V*₁₂ > *V*₁ + *V*₂) to complementary substrate cofeeding. While our ¹³C labelling experiments showed the roles of glucose and gluconate in ATP and cofactor synthesis, respectively, we sought to define the theoretical framework that illustrates the feasibility of this synergy. To this end, stoichiometric analysis of the different fates of individual substrates was combined with experimentally measured rates of single-substrate acetogenesis and lipogenesis. The maximum carbon, ATP and e⁻ attainable with mixed substrates were then evaluated for the two processes (see Supplementary Note). We identified that ATP and NADPH generation by glucose and gluconate doping relieved the limiting ingredients for acetate and lipid synthesis, respectively, and, in conjunction with the primary substrates, better balanced the energy and cofactor ratio requirements for reduced bioproduct synthesis (Fig. 6b).

In terms of organic carbon yield, the integrated acetogenesis-lipogenesis process converted 1 g of glucose to approximately 13 g of lipids (0.154 g lipids per g acetate × approximately 82 g acetate per g glucose) by extensive CO₂ use. Increasing the mass transfer rates of gases improves H₂ (and CO₂) use efficiency; it has been reported that approximately 95% of supplied H₂ can be used by commercial CO₂-fixing microbes^{30,31}. By continuously converting CO₂ and H₂ to lipids via coordinated acetogenesis and lipogenesis, 38% of energy from H₂ was stored as lipids and 14% as yeast biomass (Fig. 6c). Nearly all carbons (approximately 99%) in lipids originated from CO₂.

To further explore the potential of our synergistic cofeeding approach, we applied the stoichiometric analysis to other acetyl-CoA-derived products and determined the gains in productivities

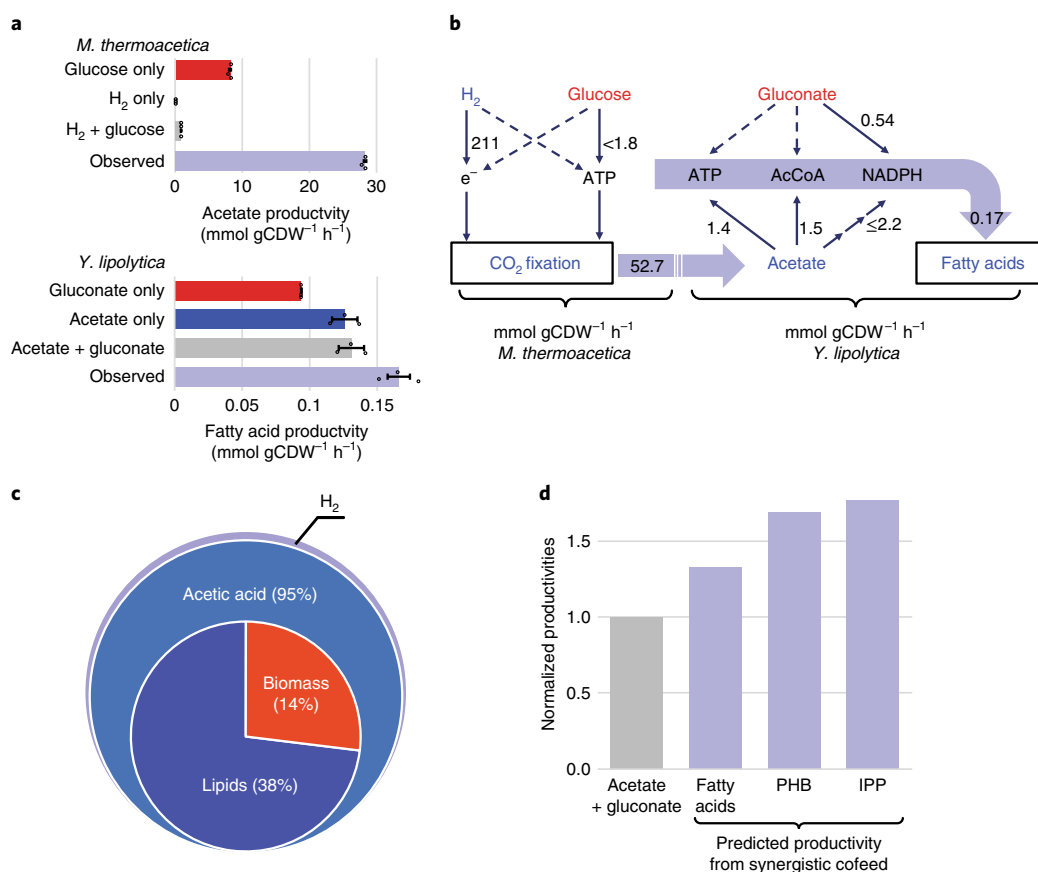


Fig. 6 | Synergy and coordination of substrate cofeeding accelerate the conversion of CO₂ and H₂ into lipids. **a**, Glucose and gluconate doping resulted in synergy ('observed') that accelerated acetogenesis and lipogenesis beyond the linear extrapolation of additional carbon supplement ('H₂ + gluconate' and 'Acetate + gluconate'). The centre and error bars represent the mean \pm s.e.m. ($n=3$ biologically independent samples). Individual data points for each biological replicate are shown as circles. **b**, The maximum CO₂ fixation and fatty acid production rates were attained by cofeeding glucose and gluconate in limiting quantities. Stoichiometric analysis of metabolic requirements and burdens revealed the key role of glucose and gluconate in generating ATP and NADPH. The dashed arrows denote negligible contributions. **c**, In terms of energy yield, 95% of H₂ energy can be stored as acetate by *M. thermoacetica* and 55% of acetate energy can be stored as lipids and biomass by *Y. lipolytica*. Coordination of acetogenesis and lipogenesis enabled storage of 38% of H₂ energy as lipids and 14% as biomass. **d**, The cofeeding approach can also be applied to synthesizing other products with predicted synergistic productivity that exceeds the sum of individual substrate productivities. IPP, isopentenyl pyrophosphate; PHB, poly-3-hydroxybutyrate.

(Fig. 6d and Supplementary Note). Similar to the results for fatty acids, the model predicted synergy between the substrate pair in producing other reduced compounds, such as poly-3-hydroxybutyrate (PHB) and isopentenyl pyrophosphate (IPP, the precursor of isoprenoids), leading to increases in productivities over the extrapolated sum ($V_{12} > V_1 + V_2$). Therefore, our synergistic substrate cofeeding strategy may stimulate conversion of CO₂ into a wide array of advanced bioproducts.

Discussion

One of the greatest biotechnological challenges is engineering metabolism. Current engineering efforts often focus on funnelling metabolic fluxes through product synthesis pathways via assembling various gene pools and knocking out competing pathways with existing genetic tools³². In addition, most processes start from sugars as the sole substrate, which inherently causes some metabolic intermediates to be out of balance and surplus components to be wasted because of the differences in chemical properties between substrate and product. This further necessitates the use of genetic engineering for flux rewiring to achieve industrially relevant production metrics. Such approaches set a limit on the choice of microbial hosts based on genetic manipulability; existing strategies are not generalizable to all organisms.

In the present study, we presented the potential of synergistic substrate cofeeding as a generalizable method and a more effective starting point for bioproduct synthesis. Importantly, we overcame the difficulties that arise due to organisms' preferential substrate use. Controlled continuous feeding of a preferred substrate as a metabolic dopant did not inhibit the consumption of the less favoured substrate. Using this approach, we enhanced the use of CO₂ and acetate, which are typically the end products of metabolism and therefore least preferred by organisms. This was demonstrated in both *M. thermoacetica* and *Y. lipolytica*, two organisms with distinct metabolism and genetic manipulability, using various substrate pairs (glucose and H₂/CO₂ as well as acetate and gluconate). Correspondingly, we expect this design to be widely applicable to other substrates and organisms.

Surprisingly, substrate cofeeding synergistically enhanced product synthesis. In both cases, the total product carbon flux resulting from co-utilized substrates exceeded the sum of the individual substrate fluxes ($V_{12} > V_1 + V_2$ where V represents the productivity on either substrate (subscript 1 or 2) or both substrates (subscript 12)). However, previous experimental efforts and models describing mixed substrate use have shown sublinear productivity enhancements ($V_{12} > V_1$ or V_2 but $V_{12} < V_1 + V_2$) and overlooked this synergistic effect^{11,33,34}. The synergistic cofeeding scheme reported in

this study goes beyond ‘sacrificing’ a secondary substrate to provide energetic gains for the primary substrate. In our case, we found that, under carefully controlled but easy to implement conditions, the two substrates can have a distinct mode of interaction, allowing them to balance fluxes across the entire metabolic network, thus achieving substantially higher productivities than previous mixed substrate fermentation efforts. Importantly, the observed substantial enhancements in CO₂ and acetate reduction metabolism required only minor addition of ‘valuable’ glucose and gluconate, and the productivity gain outweighed the ‘cost’ of the dopants.

To understand how the dopant substrates achieve such efficiency in enhancing reductive metabolism, we also elucidated the underlying mechanisms. Our stoichiometric analysis of metabolic requirements and burdens suggested that glucose and gluconate as dopant substrates could indeed complement ATP and NADPH generation, alleviating the limitations seen in acetogenesis and lipogenesis, respectively. Tracing ¹³C-labelled glucose and gluconate revealed that nearly all of glucose and gluconate were used locally within glycolysis and the PPP. Hence, cells used these substrates almost exclusively for ATP and NADPH production, respectively. We identified pyruvate kinase (PEP + ADP → pyruvate + ATP) in *M. thermoacetica* and the pentose cycle (6PG → ribose 5-phosphate (R5P) → F6P → G6P → 6PG + 2 NADPH) in *Y. lipolytica* to be important cofactor-generating steps. In particular, activating pyruvate kinase by cofeeding glucose solved the challenge of slow CO₂ fixation, which is due to ATP-limited metabolism in autotrophic fermentation^{31,35}. Activating the pentose cycle by cofeeding gluconate solved the challenge of limited NADPH production through oxidative PPP in acetate-fed cells. Therefore, we rewired metabolism without genetic engineering through synergistic cofeeding.

Akin to the widespread application of dopants in the electronics industry to enhance material properties, we envision the use of dopant substrates in synergistic cofeeding becoming valuable in a wide array of biotechnological applications. Our demonstration of CO₂/H₂-to-acetate-to-lipids conversion at high productivity (up to 2.3 g CDW⁻¹ h⁻¹ CO₂ fixation) and energetic efficiency (38% energy yield) serves as an exemplary renewable energy storage strategy, which uses substrates that do not interfere with the food supply. Since acetate is closely related to acetyl-CoA, a focal point in many metabolic pathways, other acetate-based processes applying proper doping substrates could enable rapid synthesis of a wide repertoire of bioproducts, such as fatty acid-derived oleochemicals³⁶ and mevalonate pathway-derived natural products³⁷. By coupling this to glucose-doped acetogenesis, CO₂ could become the initial feedstock for all subsequent acetate-driven processes, benefiting both the environment and carbon economy. With process optimization and scale-up, the productivities reported in this study could potentially enable these CO₂-based biosynthetic processes to be market-competitive. Therefore, the findings presented in this article contribute to various fields ranging from fundamental metabolic control theory to metabolic engineering to CO₂ use.

Finally, metabolic enhancement by cofeeding superior substrates is not limited to CO₂- and acetate-based fermentations. The imbalance of carbon building blocks, cofactors and energy with regard to the desired product requirement can also be seen in many other single-substrate bioconversions. In these cases, identification of complementary substrates and implementation of controlled dopant substrate cofeeding would optimally coordinate pathway use for superior biosynthesis. Consequently, substrates previously considered infeasible for industrial bioprocesses because of limited productivity may be well suited as economically and technologically viable feedstocks³⁸.

Methods

Strains and culture conditions. *Y. lipolytica* strains based on the ACC-DGA strain (MTYL065)³⁹ were pre-cultured at 30 °C in 14 ml test tubes containing

yeast extract–peptone–dextrose media (20 g l⁻¹ glucose, 20 g l⁻¹ peptone and 10 g l⁻¹ yeast extract). After 24 h, 1 ml of culture was transferred to a shake flask containing 40 ml of acetate media (50 g l⁻¹ sodium acetate, 1.7 g l⁻¹ yeast nitrogen base without amino acids and ammonium sulfate and 1.34 g l⁻¹ ammonium sulfate). The shake flask culture was carried out for 24 h to adapt the cells to acetate. Afterwards, the cells were pelleted at 18,000g for 5 min, washed once with acetate media and used for inoculation at an initial optical density OD₆₀₀ of 0.05 for all *Y. lipolytica* experiments.

Mixed substrate batch cultures were carried out in shake flasks with 40 ml of acetate media except that 6 mol% of the total carbon from acetate was replaced with the supplemental substrate (glucose, fructose, glycerol or gluconate). Continuous fed-batch supplementation cultures were carried out in 250 ml bioreactors (Applikon Biotechnology) with a 150 ml working volume. Acetate media were used under batch conditions while the supplemented substrate was continuously fed at a rate of 0.13 mmol C h⁻¹. For the acetate-only control, the supplemented substrate was replaced with acetate and fed at the same rate to ensure that cells had equal amounts of carbon substrate throughout all conditions. All bioreactor cultures were carried out at 30 °C, pH 7.0 (controlled with 10 wt% sulfuric acid) and 0.21 min⁻¹ air sparging. The dissolved oxygen levels were controlled at 20% during the growth phase and approximately 2% during the lipogenic phase for optimal lipid production and minimal citrate excretion⁴. For the gluconate ¹³C tracing experiments, natural gluconate in the supplementation feed stream was replaced with [U-¹³C₆]-gluconate (99%; Cambridge Isotope Laboratories).

In all *Y. lipolytica* experiments having gluconate as a substrate, an ACC-DGA strain overexpressing its native gluconate kinase under the *TEF_{in}* promoter was used. The expression of *TEF_{in}*-gluconate kinase was performed through genome integration. This was to ensure that gluconate uptake and incorporation into central carbon metabolism was not inhibited by inadequate levels of the kinase. All other experiments were performed using the same ACC-DGA strain with an empty control vector integrated into the genome. Overexpressing gluconate kinase did not have any appreciable effects on the strain's capability to produce lipids on acetate, as shown in Supplementary Fig. 9.

M. thermoacetica (catalogue nos. 39073 and 49707; ATCC) were cultured in Balch-type tubes containing culture medium with 8 g l⁻¹ glucose, 7.5 g l⁻¹ NaHCO₃, 7 g l⁻¹ KH₂PO₄, 5.5 g l⁻¹ K₂HPO₄, 2 g l⁻¹ (NH₄)₂SO₄, 0.5 g l⁻¹ MgSO₄ • 7H₂O, 0.3 g l⁻¹ cysteine, 0.02 g l⁻¹ CaCl₂ • 2H₂O, 1% (v/v) trace minerals (ATCC MD-TMS) and 1% (v/v) vitamins (ATCC MD-VS) at 55 °C, pH 6.8. Cysteine scavenged residual dissolved oxygen in the medium⁴⁰. The headspace was pressurized to either 170 kPa with CO₂ or 240 kPa with 80:20 H₂/CO₂. For the ¹³C tracing experiments, natural glucose was replaced with [U-¹³C₆]-glucose (99%; Cambridge Isotope Laboratories) and the headspace was pressurized to 170 kPa with natural CO₂. The Balch-tube cultures were incubated inside a strictly anoxic glovebox with magnetic stirring.

For the bioreactor experiments, *M. thermoacetica* (catalogue no. 49707; ATCC) was cultured in a strictly anoxic vessel with pH and temperature control set to 6.6 (using 10 M sodium hydroxide) and 55 °C. Low-glucose, but otherwise identical culture media, were fed as follows (media glucose concentrations and feed rates): 0.25 g l⁻¹ at 11.5 ml h⁻¹; 0.25 g l⁻¹ at 9.1 ml h⁻¹; 0.25 g l⁻¹ at 6.9 ml h⁻¹; 0.25 g l⁻¹ at 4.3 ml h⁻¹; 0.25 g l⁻¹ at 2.3 ml h⁻¹; 0.25 g l⁻¹ at 1.2 ml h⁻¹; and 0.13 g l⁻¹ at 1.2 ml h⁻¹. The rate of effluent was the same to keep the culture volume constant at 135 ml. H₂ and CO₂ were mixed at 60:40 and sparged into the culture at 200 ml min⁻¹. The headspace pressure was maintained at 130 kPa. All the data and conditions are shown in Supplementary Table 5.

Metabolite extraction and measurement. To extract metabolites, *Y. lipolytica* cells were collected during the exponential and lipogenic phases. Cells were filtered on 0.45 µm nylon membrane filters and immediately transferred to a pre-cooled 40:40:20 acetonitrile/methanol/water solution. After 20 min at -20 °C, the filters were washed and the extracts were moved to Eppendorf tubes. The samples were then centrifuged for 5 min and the supernatants were dried under nitrogen.

In the mid-exponential phase, the *M. thermoacetica* cultures were collected from Balch-type tubes using syringes inside the anaerobic glovebox. Immediately after, cellular metabolism was quenched and metabolites were extracted by quickly transferring filtered cells (on a 0.2 µm nylon membrane filter) to plates containing pre-cooled 80% acetonitrile on ice⁴¹. After 20 min at 4 °C, the membrane filters were washed and the metabolite extracts were moved to Eppendorf tubes. The supernatants were obtained after 5 min of centrifugation and lyophilized.

Dried samples were resuspended in high-performance liquid chromatography (HPLC)-grade water for the LC-MS analysis. These samples were analysed on a Dionex UltiMate 3000 UPLC system (Thermo Fisher Scientific) with a ZIC-pHILIC (5 µm polymer particle) 150 × 2.1 mm column (Merck) coupled to a Q Exactive Orbitrap Mass Spectrometer (Thermo Fisher Scientific) by electrospray ionization. With 20 mM ammonium carbonate, 0.1% ammonium hydroxide as solvent A and acetonitrile as solvent B, the chromatographic gradient was run at a flow rate of 0.150 ml min⁻¹ as a linear gradient from 80% B to 20% B between 0 and 20 min, a linear gradient from 20% B to 80% B between 20 and 20.5 min and 80% B held from 20.5 to 28 min. The temperature of the column and autosampler tray was 25 °C and 4 °C, respectively. The mass spectrometer was operated in polarity switching mode scanning a range of 70–1,000 m/z. The resolving power was set to 70,000 for the ¹³C labelling experiments. With retention times determined by

authenticated standards, the resulting mass spectra and chromatograms were identified and processed with the MAVEN software v.682 (ref. 43). To obtain the labelling information of cellular bicarbonate and acetate, the labelling of the carbamoyl group was obtained by comparing (that is, computing the inverse Cauchy product) citrulline to ornithine, and the labelling of the acetyl group was obtained by comparing *N*-acetylglutamate to glutamate.

Substrate uptake and product secretion measurement. For *Y. lipolytica*, 1 ml of culture was taken at each time point for media and CDW analysis. The cells were centrifuged at 18,000g for 10 min and the supernatant was subsequently extracted, filtered (0.2 µm syringe filters) and analysed using HPLC. The cell pellet was then washed once with 1 ml water to remove residual media components and dried in a 60 °C oven until its mass remained unchanged. This mass was taken to be the CDW per ml of culture. As for lipids, a small volume was extracted from the culture such that it contained approximately 1 mg of CDW. The supernatant was discarded after centrifugation at 18,000g for 10 min; 100 µl of an internal standard containing 2 mg ml⁻¹ methyl tridecanoate (Sigma-Aldrich) and 2 mg ml⁻¹ glyceryl triheptadecanoate (Sigma-Aldrich) in hexane was added to each sample. Transesterification was then carried out in 500 µl 0.5 N sodium methoxide solutions with continuous vortexing at 1,200 r.p.m. for 60 min. Afterwards, 40 µl of 98% sulfuric acid was added to neutralize the pH and 500 µl of hexane was used for extraction. Additional vortexing at 1,200 r.p.m. for 30 min was carried out and centrifugation at 6,000g for 1 min was performed to remove cellular debris. The top hexane layer was used for analysis on a gas chromatography with flame ionization detector (GC-FID) system (Agilent). All *Y. lipolytica* specific rate data were normalized to the lipid-free CDW, which was the difference between the measured CDW and the lipid titre.

For media analysis in *M. thermoacetica* cultures, small aliquots of the cultures were collected with syringes inside the anaerobic glovebox during their exponential phase. Filtered media samples (0.2 µm syringe filters) were analysed using a YSI Biochemistry Analyzer (Xylem Analytics) for glucose and HPLC for acetate and formate along with other potential products (for example, lactate and ethanol). Culture density was measured by spectrophotometry (0.45 gCDW l⁻¹ OD₆₀₀⁻¹) at the time of sampling. The rates of substrate uptake and product secretion were determined using the rates at which substrates, products and culture density change over time. The carbon output rate for biomass was determined using the growth rate and elemental biomass composition of CH_{2.08}O_{0.53}N_{0.24} (ref. 43). The net CO₂ fixation rates were calculated based on the measured acetate and biomass carbon production rates less the corresponding measured glucose carbon consumption rates. The fraction of e⁻ derived from H₂ was inferred from the fraction of acetate and biomass carbons generated from net CO₂ fixation since the average oxidation state of acetate and biomass carbons is nearly the same as that of glucose.

For HPLC, a 10 µl sample was injected into an Agilent 1200 HPLC system coupled to a G1362 Refractive Index Detector (Agilent Technologies). An HPX-87H column (Bio-Rad Laboratories) was used for separation with 14 mM sulfuric acid as the mobile phase flowing at 0.7 ml min⁻¹. For GC-FID, 1 µl of sample was injected at a split ratio of 50:1 into an Agilent 7890B GC-FID system coupled to a J&W HP-INNOWax capillary column (Agilent Technologies). The column was held at a constant temperature of 200 °C with helium as the carrier gas (1.5 ml min⁻¹). The injection and FID temperatures were set to 260 °C.

Headspace gas measurement. After collection of the *M. thermoacetica* cultures from the Balch-type tubes inside the anaerobic glovebox for intracellular and extracellular metabolite analysis, the empty Balch-type tubes containing only the headspace gas were stored at 4 °C until gas chromatography–mass spectrometry analysis. To measure CO₂ isotope labelling, 100 µl of the headspace sample were collected from each tube with a gastight syringe and injected into a multimode inlet, which was maintained at 180 °C, with a split ratio of 10:1. Samples were analysed on a 7890A GC system with a 60 m GS-GasPro (0.320 mm diameter) column coupled with a 5975C quadrupole mass spectrometer (Agilent Technologies). The oven was kept at 90 °C for 3 min before heating to 260 °C at 45 °C min⁻¹ and held at 260 °C for 1 min.

Flux balance analysis and isotope-tracing flux analysis. The *M. thermoacetica* model based on the published genome-scale metabolic reconstruction⁴⁴ was employed for the constraint-based flux analysis (see Supplementary Note). Among the feasible metabolic flux distributions that satisfy steady-state mass balance and nutrient availability constraints, optimal solutions that maximize/minimize objective functions were obtained using the COBRA Toolbox v.2.0 and Gurobi solver v.7.0.1 (64 bit)⁴⁵. To determine CO₂ use capability, the objective was to maximize CO₂ consumption, or equivalently, minimize CO₂ production. To determine the growth potential using H₂ as the energy source, the objective was to maximize biomass production (that is, cell growth). The substrate uptake and product secretion rate constraints were selected based on experimental or previously reported values.

To determine flux distributions, isotopomer mass balance constraints were also imposed based on the ¹³C labelling results. For this purpose, the metabolic networks including glycolysis and PPP for *Y. lipolytica* as well as lower glycolysis, TCA cycle, anaplerosis and the reductive acetyl-CoA and Ser/Gly pathways for

M. thermoacetica were constructed with carbon atom mapping. Labelling of the following metabolites was simulated with the elementary metabolite unit framework⁴⁶: for *Y. lipolytica*, G6P, F6P, 3-phosphoglyceric acid, sedoheptulose 7-phosphate, 6PG, R5P, PEP and pyruvate (Supplementary Table 1); for *M. thermoacetica*, 3-phosphoglyceric acid, PEP, Ala, acetyl-CoA, Ser, Gly, Asp, Glu and CO₂ (Supplementary Table 3).

The flux distribution that best simulated metabolite labelling and the uptake/secretion rates was found by minimizing the variance weighted sum of squared residuals between simulation and experiment, as shown in equation (1):

$$\min_{\mathbf{v}} \sum \left(\frac{\mathbf{iso}_{\text{exp}} - \mathbf{iso}(\mathbf{v})}{s_{\text{iso}}} \right)^2 + \sum \left(\frac{\mathbf{v}_{\text{exp}} - \mathbf{v}}{s_{\mathbf{v}}} \right)^2$$

\mathbf{v} and $\mathbf{iso}(\mathbf{v})$ denote in vector form the metabolic flux distribution and the simulated ¹³C labelling of metabolites as a function of \mathbf{v} . \mathbf{v}_{exp} and $\mathbf{iso}_{\text{exp}}$ denote measured fluxes and measured metabolite labelling; $s_{\mathbf{v}}$ and s_{iso} represent the measurement's s.d. The 95% confidence interval for each best-fit flux was obtained by searching for the minimum and maximum flux values that increase the minimum sum of squared residuals by less than the χ^2 cut-off (1 d.f.) of 3.84 (ref. 47).

Reporting Summary. Further information on the research design is available in the Nature Research Reporting Summary linked to this article.

Data availability

The data that support the findings of this study are available in the Supplementary Files and from the corresponding author upon request.

Code availability

The code for the metabolic flux and free energy analysis is available on the GitHub public repository at https://github.com/jopark/moorella_yarrowia. The data that support the findings of this study are available in the Supplementary Files and from the corresponding author upon request.

Received: 10 August 2018; Accepted: 13 May 2019;
Published online: 14 June 2019

References

- Ledesma-Amaro, R. & Nicaud, J. M. Metabolic engineering for expanding the substrate range of *Yarrowia lipolytica*. *Trends Biotechnol.* **34**, 798–809 (2016).
- Atsumi, S., Hanai, T. & Liao, J. C. Non-fermentative pathways for synthesis of branched-chain higher alcohols as biofuels. *Nature* **451**, 86–89 (2008).
- Xue, Z. et al. Production of omega-3 eicosapentaenoic acid by metabolic engineering of *Yarrowia lipolytica*. *Nat. Biotechnol.* **31**, 734–740 (2013).
- Qiao, K. J., Wasylenko, T. M., Zhou, K., Xu, P. & Stephanopoulos, G. Lipid production in *Yarrowia lipolytica* is maximized by engineering cytosolic redox metabolism. *Nat. Biotechnol.* **35**, 173–177 (2017).
- Kita, A. et al. Development of genetic transformation and heterologous expression system in carboxydophilic thermophilic acetogen *Moorella thermoacetica*. *J. Biosci. Bioeng.* **115**, 347–352 (2013).
- Monod, J. Recherches sur la Croissance des Cultures Bactériennes. (Hermann: 1942).
- Aristilde, L., Lewis, I. A., Park, J. O. & Rabinowitz, J. D. Hierarchy in pentose sugar metabolism in *Clostridium acetobutylicum*. *Appl. Environ. Microbiol.* **81**, 1452–1462 (2015).
- Görke, B. & Stülke, J. Carbon catabolite repression in bacteria: many ways to make the most out of nutrients. *Nat. Rev. Microbiol.* **6**, 613–624 (2008).
- Bren, A. et al. Glucose becomes one of the worst carbon sources for *E. coli* on poor nitrogen sources due to suboptimal levels of cAMP. *Sci. Rep.* **6**, 24834 (2016).
- Joshua, C. J., Dahl, R., Benke, P. I. & Keasling, J. D. Absence of diauxia during simultaneous utilization of glucose and xylose by *Sulfolobus acidocaldarius*. *J. Bacteriol.* **193**, 1293–1301 (2011).
- Hermesen, R., Okano, H., You, C., Werner, N. & Hwa, T. A growth-rate composition formula for the growth of *E. coli* on co-utilized carbon substrates. *Mol. Syst. Biol.* **11**, 801 (2015).
- Kanno, M., Carroll, A. L. & Atsumi, S. Global metabolic rewiring for improved CO₂ fixation and chemical production in cyanobacteria. *Nat. Commun.* **8**, 14724 (2017).
- Martinez, K. et al. Couitilization of glucose and glycerol enhances the production of aromatic compounds in an *Escherichia coli* strain lacking the phosphoenolpyruvate: carbohydrate phosphotransferase system. *Microb. Cell Fact.* **7**, 1 (2008).
- Meyer, F. et al. Methanol-essential growth of *Escherichia coli*. *Nat. Commun.* **9**, 1508 (2018).
- Garcia Sanchez, R. et al. Improved xylose and arabinose utilization by an industrial recombinant *Saccharomyces cerevisiae* strain using evolutionary engineering. *Biotechnol. Biofuels* **3**, 13 (2010).

16. Kim, S. M. et al. Simultaneous utilization of glucose and xylose via novel mechanisms in engineered *Escherichia coli*. *Metab. Eng.* **30**, 141–148 (2015).
17. Jones, S. W. et al. CO₂ fixation by anaerobic non-photosynthetic mixotrophy for improved carbon conversion. *Nat. Commun.* **7**, 12800 (2016).
18. Bowes, G., Ogren, W. L. & Hageman, R. H. Light saturation, photosynthesis rate, RuDP carboxylase activity, and specific leaf weight in soybeans grown under different light intensities. *Crop Sci.* **12**, 77 (1972).
19. Xu, J., Liu, N., Qiao, K., Vogt, S. & Stephanopoulos, G. Application of metabolic controls for the maximization of lipid production in semicontinuous fermentation. *Proc. Natl Acad. Sci. USA* **114**, E5308–E5316 (2017).
20. Ratledge, C. & Wynn, J. P. The biochemistry and molecular biology of lipid accumulation in oleaginous microorganisms. *Adv. Appl. Microbiol.* **51**, 1–51 (2002).
21. Qiao, K. et al. Engineering lipid overproduction in the oleaginous yeast *Yarrowia lipolytica*. *Metab. Eng.* **29**, 56–65 (2015).
22. Fontanille, P., Kumar, V., Christophe, G., Nouaille, R. & Larroche, C. Bioconversion of volatile fatty acids into lipids by the oleaginous yeast *Yarrowia lipolytica*. *Bioresour. Technol.* **114**, 443–449 (2012).
23. Liu, N., Qiao, K. & Stephanopoulos, G. ¹³C metabolic flux analysis of acetate conversion to lipids by *Yarrowia lipolytica*. *Metab. Eng.* **38**, 86–97 (2016).
24. Gancedo, J. M. Carbon catabolite repression in yeast. *Eur. J. Biochem.* **206**, 297–313 (1992).
25. Casazza, J. P. & Veech, R. L. The interdependence of glycolytic and pentose cycle intermediates in ad libitum fed rats. *J. Biol. Chem.* **261**, 690–698 (1986).
26. Ragsdale, S. W. & Pierce, E. Acetogenesis and the Wood–Ljungdahl pathway of CO₂ fixation. *Biochim. Biophys. Acta* **1784**, 1873–1898 (2008).
27. Mall, A. et al. Reversibility of citrate synthase allows autotrophic growth of a thermophilic bacterium. *Science* **359**, 563–567 (2018).
28. Nunoura, T. et al. A primordial and reversible TCA cycle in a facultatively chemolithoautotrophic thermophile. *Science* **359**, 559–563 (2018).
29. Schuchmann, K. & Müller, V. Autotrophy at the thermodynamic limit of life: a model for energy conservation in acetogenic bacteria. *Nat. Rev. Microbiol.* **12**, 809–821 (2014).
30. Daniell, J., Köpke, M. & Simpson, S. Commercial biomass syngas fermentation. *Energies* **5**, 5372–5417 (2012).
31. Hu, P., Rismani-Yazdi, H. & Stephanopoulos, G. Anaerobic CO₂ fixation by the acetogenic bacterium *Moorella thermoacetica*. *AIChE J.* **59**, 3176–3183 (2013).
32. Blazeck, J. et al. Harnessing *Yarrowia lipolytica* lipogenesis to create a platform for lipid and biofuel production. *Nat. Commun.* **5**, 3131 (2014).
33. Babel, W., Brinkmann, U. & Müller, R. H. The auxiliary substrate concept: an approach for overcoming limits of microbial performances. *Acta Biotechnol.* **13**, 211–242 (1993).
34. Babel, W. The auxiliary substrate concept: from simple considerations to heuristically valuable knowledge. *Eng. Life Sci.* **9**, 285–290 (2009).
35. Daniel, S. L., Hsu, T., Dean, S. I. & Drake, H. L. Characterization of the H₂- and CO-dependent chemolithotrophic potentials of the acetogens *Clostridium thermoacetatum* and *Acetogenium kivui*. *J. Bacteriol.* **172**, 4464–4471 (1990).
36. Ledesma-Amaro, R., Dulermo, R., Niehus, X. & Nicaud, J. M. Combining metabolic engineering and process optimization to improve production and secretion of fatty acids. *Metab. Eng.* **38**, 38–46 (2016).
37. Martin, V. J., Pitera, D. J., Withers, S. T., Newman, J. D. & Keasling, J. D. Engineering a mevalonate pathway in *Escherichia coli* for production of terpenoids. *Nat. Biotechnol.* **21**, 796–802 (2003).
38. Haynes, C. A. & Gonzalez, R. Rethinking biological activation of methane and conversion to liquid fuels. *Nat. Chem. Biol.* **10**, 331–339 (2014).
39. Tai, M. & Stephanopoulos, G. Engineering the push and pull of lipid biosynthesis in oleaginous yeast *Yarrowia lipolytica* for biofuel production. *Metab. Eng.* **15**, 1–9 (2013).
40. Michaelis, L. & Guzman Barron, E. S. Oxidation-reduction systems of biological significance. II. Reducing effect of cysteine induced by free metals. *J. Biol. Chem.* **81**, 29–40 (1929).
41. Rabinowitz, J. D. & Kimball, E. Acidic acetonitrile for cellular metabolome extraction from *Escherichia coli*. *Anal. Chem.* **79**, 6167–6173 (2007).
42. Clasquin, M. F., Melamud, E. & Rabinowitz, J. D. LC–MS data processing with MAVEN: a metabolomic analysis and visualization engine. *Curr. Protoc. Bioinformatics* **Chapter 14**, Unit14.11 (2012).
43. Tracy, B. P., Jones, S. W., Fast, A. G., Indurthi, D. C. & Papoutsakis, E. T. Clostridia: the importance of their exceptional substrate and metabolite diversity for biofuel and biorefinery applications. *Curr. Opin. Biotechnol.* **23**, 364–381 (2012).
44. Islam, M. A., Zengler, K., Edwards, E. A., Mahadevan, R. & Stephanopoulos, G. Investigating *Moorella thermoacetica* metabolism with a genome-scale constraint-based metabolic model. *Integr. Biol. (Camb.)* **7**, 869–882 (2015).
45. Schellenberger, J. et al. Quantitative prediction of cellular metabolism with constraint-based models: the COBRA Toolbox v2.0. *Nat. Protoc.* **6**, 1290–1307 (2011).
46. Antoniewicz, M. R., Kelleher, J. K. & Stephanopoulos, G. Elementary metabolite units (EMU): a novel framework for modeling isotopic distributions. *Metab. Eng.* **9**, 68–86 (2007).
47. Antoniewicz, M. R., Kelleher, J. K. & Stephanopoulos, G. Determination of confidence intervals of metabolic fluxes estimated from stable isotope measurements. *Metab. Eng.* **8**, 324–337 (2006).

Acknowledgements

The authors would like to thank C. Lewis and E. Freinkman for their help with the LC–MS. This research was supported by the U.S. Department of Energy grant nos. DE-AR0000433, DE-SC0008744 and DE-SC0012377, as well as a Mobility Plus Fellowship no. 1284/MOB/IV/2015/0.

Author contributions

J.O.P., N.L. and G.S. designed the study and wrote the paper. J.O.P., N.L. and K.M.H. performed the experiments and flux analysis. J.O.P., N.L., B.M.W. and C.V. developed the methods for the LC–MS and gas chromatography–mass spectrometry. J.O.P., N.L., D.F.E. and J.X. designed the bioreactors. J.O.P. and M.A.I. developed the updated metabolic model. J.O.P., N.L., K.Q., Z.L., P.R.G. and G.S. analysed the data.

Competing interests

The authors declare no competing interests.

Additional information

Supplementary information is available for this paper at <https://doi.org/10.1038/s42255-019-0077-0>.

Reprints and permissions information is available at www.nature.com/reprints.

Correspondence and requests for materials should be addressed to G.S.

Peer review information: Primary Handling Editor: Ana Mateus.

Publisher's note: Springer Nature remains neutral with regard to jurisdictional claims in published maps and institutional affiliations.

© The Author(s), under exclusive licence to Springer Nature Limited 2019

Reporting Summary

Nature Research wishes to improve the reproducibility of the work that we publish. This form provides structure for consistency and transparency in reporting. For further information on Nature Research policies, see [Authors & Referees](#) and the [Editorial Policy Checklist](#).

Statistics

For all statistical analyses, confirm that the following items are present in the figure legend, table legend, main text, or Methods section.

n/a Confirmed

- | | | |
|-------------------------------------|-------------------------------------|--|
| <input type="checkbox"/> | <input checked="" type="checkbox"/> | The exact sample size (n) for each experimental group/condition, given as a discrete number and unit of measurement |
| <input type="checkbox"/> | <input checked="" type="checkbox"/> | A statement on whether measurements were taken from distinct samples or whether the same sample was measured repeatedly |
| <input checked="" type="checkbox"/> | <input type="checkbox"/> | The statistical test(s) used AND whether they are one- or two-sided
<i>Only common tests should be described solely by name; describe more complex techniques in the Methods section.</i> |
| <input checked="" type="checkbox"/> | <input type="checkbox"/> | A description of all covariates tested |
| <input checked="" type="checkbox"/> | <input type="checkbox"/> | A description of any assumptions or corrections, such as tests of normality and adjustment for multiple comparisons |
| <input type="checkbox"/> | <input checked="" type="checkbox"/> | A full description of the statistical parameters including central tendency (e.g. means) or other basic estimates (e.g. regression coefficient) AND variation (e.g. standard deviation) or associated estimates of uncertainty (e.g. confidence intervals) |
| <input checked="" type="checkbox"/> | <input type="checkbox"/> | For null hypothesis testing, the test statistic (e.g. F , t , r) with confidence intervals, effect sizes, degrees of freedom and P value noted
<i>Give P values as exact values whenever suitable.</i> |
| <input checked="" type="checkbox"/> | <input type="checkbox"/> | For Bayesian analysis, information on the choice of priors and Markov chain Monte Carlo settings |
| <input checked="" type="checkbox"/> | <input type="checkbox"/> | For hierarchical and complex designs, identification of the appropriate level for tests and full reporting of outcomes |
| <input checked="" type="checkbox"/> | <input type="checkbox"/> | Estimates of effect sizes (e.g. Cohen's d , Pearson's r), indicating how they were calculated |

Our web collection on [statistics for biologists](#) contains articles on many of the points above.

Software and code

Policy information about [availability of computer code](#)

Data collection

MATLAB 2014a was used to run the linear optimization model and all flux analysis. The custom code in MATLAB used for free energy calculation and flux analysis can be found at github.com/jopark/moorella_yarrowia

Data analysis

MATLAB 2014a and Microsoft Excel 2016 were used to process and analyze all data. Additionally, MAVEN (<http://genomics-pubs.princeton.edu/mzroll/index.php>) was used to process data collected from LC-MS measurements. MATLAB 2014a was used to run the linear optimization model and all flux analysis. The custom code in MATLAB used for free energy calculation and flux analysis can be found at github.com/jopark/moorella_yarrowia

For manuscripts utilizing custom algorithms or software that are central to the research but not yet described in published literature, software must be made available to editors/reviewers. We strongly encourage code deposition in a community repository (e.g. GitHub). See the Nature Research [guidelines for submitting code & software](#) for further information.

Data

Policy information about [availability of data](#)

All manuscripts must include a [data availability statement](#). This statement should provide the following information, where applicable:

- Accession codes, unique identifiers, or web links for publicly available datasets
- A list of figures that have associated raw data
- A description of any restrictions on data availability

The code for metabolic flux and free energy analysis is available on the GitHub public repository: https://github.com/jopark/moorella_yarrowia. The data that support the findings of this study are available in the Supplementary Information and from the corresponding author upon request.

Field-specific reporting

Please select the one below that is the best fit for your research. If you are not sure, read the appropriate sections before making your selection.

Life sciences Behavioural & social sciences Ecological, evolutionary & environmental sciences

For a reference copy of the document with all sections, see [nature.com/documents/nr-reporting-summary-flat.pdf](https://www.nature.com/documents/nr-reporting-summary-flat.pdf)

Life sciences study design

All studies must disclose on these points even when the disclosure is negative.

Sample size	A sample size of 3 biological replicates were chosen for all experiments. As microbial culture experiments are well controlled, 3 biological replicates are sufficient. No sample size calculation was performed.
Data exclusions	No data were excluded from analysis.
Replication	All experiments were repeated at least twice and all attempts at replication were successful.
Randomization	All samples were measured randomly on the corresponding instruments. For cell culture, single colonies of strains were selected at random to initiate the culture.
Blinding	Blinding was not necessary since measurements did not involve bias from the experimentalist.

Reporting for specific materials, systems and methods

We require information from authors about some types of materials, experimental systems and methods used in many studies. Here, indicate whether each material, system or method listed is relevant to your study. If you are not sure if a list item applies to your research, read the appropriate section before selecting a response.

Materials & experimental systems

n/a	Included in the study
<input checked="" type="checkbox"/>	<input type="checkbox"/> Antibodies
<input type="checkbox"/>	<input checked="" type="checkbox"/> Eukaryotic cell lines
<input checked="" type="checkbox"/>	<input type="checkbox"/> Palaeontology
<input checked="" type="checkbox"/>	<input type="checkbox"/> Animals and other organisms
<input checked="" type="checkbox"/>	<input type="checkbox"/> Human research participants
<input checked="" type="checkbox"/>	<input type="checkbox"/> Clinical data

Methods

n/a	Included in the study
<input checked="" type="checkbox"/>	<input type="checkbox"/> ChIP-seq
<input checked="" type="checkbox"/>	<input type="checkbox"/> Flow cytometry
<input checked="" type="checkbox"/>	<input type="checkbox"/> MRI-based neuroimaging

Eukaryotic cell lines

Policy information about [cell lines](#)

Cell line source(s)	All <i>Yarrowia lipolytica</i> strains used in this study was based on the parental strain po1g, which was purchased from Yeastern Biotech.
Authentication	Each <i>Yarrowia lipolytica</i> strain was confirmed by extracting genomic DNA and confirming the existence of key genes through PCR. Their proper morphology was also confirmed on agar plates and under the microscope.
Mycoplasma contamination	<i>Yarrowia lipolytica</i> strains were not tested for mycoplasma
Commonly misidentified lines (See CLAC register)	None